Depression of voltage-activated Ca^{2+} release in skeletal muscle by activation of a voltage-sensing phosphatase

Christine Berthier,[1] Candice Kutchukian,[1] Clément Bouvard,[1] Yasushi Okamura,[2] and Vincent Jacquemond[1]

[1]Centre National de la Recherche Scientifique UMR 5534, Université Lyon 1, Centre de Génétique et de Physiologie Moléculaire et Cellulaire, 69100 Villeurbanne, France

[2]Laboratory of Integrative Physiology, Graduate School of Medicine, Osaka University, Suita, Osaka 565-0871, Japan

Phosphoinositides act as signaling molecules in numerous cellular transduction processes, and phosphatidylinositol 4,5-bisphosphate (PtdIns(4,5)P_2) regulates the function of several types of plasma membrane ion channels. We investigated the potential role of PtdIns(4,5)P_2 in Ca^{2+} homeostasis and excitation–contraction (E-C) coupling of mouse muscle fibers using in vivo expression of the voltage-sensing phosphatases (VSPs) *Ciona intestinalis* VSP (Ci-VSP) or *Danio rerio* VSP (Dr-VSP). Confocal images of enhanced green fluorescent protein–tagged Dr-VSP revealed a banded pattern consistent with VSP localization within the transverse tubule membrane. Rhod-2 Ca^{2+} transients generated by 0.5-s-long voltage-clamp depolarizing pulses sufficient to elicit Ca^{2+} release from the sarcoplasmic reticulum (SR) but below the range at which VSPs are activated were unaffected by the presence of the VSPs. However, in Ci-VSP–expressing fibers challenged by 5-s-long depolarizing pulses, the Ca^{2+} level late in the pulse (3 s after initiation) was significantly lower at 120 mV than at 20 mV. Furthermore, Ci-VSP–expressing fibers showed a reversible depression of Ca^{2+} release during trains, with the peak Ca^{2+} transient being reduced by ~30% after the application of 10 200-ms-long pulses to 100 mV. A similar depression was observed in Dr-VSP–expressing fibers. Cav1.1 Ca^{2+} channel–mediated current was unaffected by Ci-VSP activation. In fibers expressing Ci-VSP and a pleckstrin homology domain fused with monomeric red fluorescent protein (PLCδ_1PH-mRFP), depolarizing pulses elicited transient changes in mRFP fluorescence consistent with release of transverse tubule–bound PLCδ_1PH domain into the cytosol; the voltage sensitivity of these changes was consistent with that of Ci-VSP activation, and recovery occurred with a time constant in the 10-s range. Our results indicate that the PtdIns(4,5)P_2 level is tightly maintained in the transverse tubule membrane of the muscle fibers, and that VSP-induced depletion of PtdIns(4,5)P_2 impairs voltage-activated Ca^{2+} release from the SR. Because Ca^{2+} release is thought to be independent from $InsP_3$ signaling, the effect likely results from an interaction between PtdIns(4,5)P_2 and a protein partner of the E-C coupling machinery.

INTRODUCTION

Muscle contraction is initiated when action potentials fired at the end-plate of the muscle cells propagate throughout the transverse tubule system and reach a region called the triad where the transverse tubule membrane comes into close apposition with two terminal cisternae of SR. There, transverse tubule depolarization triggers a conformational change of the dihydropyridine receptor (DHPR; the Cav1.1 protein), which gates open the Ca^{2+} release channel (type 1 RyR [RyR1]) present in the adjacent SR membrane, through a protein–protein conformational coupling process: Ca^{2+} gets massively released from the SR into the cytosol, which increases the concentration of Ca–troponin C complex, triggering contraction (see Ríos et al., 1992; Schneider, 1994; Melzer et al., 1995). The process is rapidly and fully reversible so that upon membrane repolarization, muscle relaxation occurs driven by ATP-fuelled SR Ca^{2+} uptake. Although the remarkable reliability of the DHPR–RyR1 coupling keeps Ca^{2+} release under the strict control of the membrane potential, there are possibilities for modulation of this process by several candidate molecules and accessory proteins (Dulhunty, 2006; Treves et al., 2009). For many of them, the physiological relevance of this modulation at the intact cell level remains unclear. Phosphatidylinositol 4,5-bisphosphate (PtdIns(4,5)P_2) is known to play a critical role in a wide diversity of cellular functions by acting either as substrate of phospholipase C to produce inositol-trisphosphate (Ins(1,4,5)P_3) and diacylglycerol, or by acting as a direct lipid messenger through interactions with specific

Correspondence to Vincent Jacquemond: vincent.jacquemond@univ-lyon1.fr

Abbreviations used in this paper: Ci-VSP, *Ciona intestinalis* voltage-sensing phosphatase; DHPR, dihydropyridine receptor; Dr-VSP, *Danio rerio* voltage-sensing phosphatase; E-C, excitation–contraction; Ins(1,4,5)P_3, inositol-trisphosphate; PtdIns(4,5)P_2, phosphatidylinositol 4,5-bisphosphate; VSP, voltage-sensing phosphatase.

The Rockefeller University Press $30.00
J. Gen. Physiol. Vol. 145 No. 4 315–330
www.jgp.org/cgi/doi/10.1085/jgp.201411309

motifs of proteins including several types of ion channels or by being the precursor of other phosphoinositide messengers with an analogous function.

In skeletal muscle, it has been generally agreed for ~20 years that there is little room for the prospect that Ins(1,4,5)P_3 plays a direct role in excitation–contraction (E-C) coupling, as recently revisited by Blaauw et al. (2012). It should be mentioned though that this does not exclude the potential for Ins(1,4,5)P_3 to be involved in Ca^{2+} signals with a physiological purpose other than contraction, either in a voltage-dependent (Casas et al., 2010; Jorquera et al., 2013) or voltage-independent manner (Tjondrokoesoemo et al., 2013). On the other hand, considering the growing number of proteins and specifically of voltage-dependent and voltage-independent ion channels that are sensitive to the PtdIns(4,5)P_2 level in the plasma membrane, it was of strong interest to investigate whether the function of the E-C coupling molecular machinery would be dependent on PtdIns(4,5)P_2 level. To this aim, we have expressed in vivo, in adult differentiated muscle fibers from mouse, a voltage-sensing phosphatase (VSP) that dephosphorylates PtdIns(4,5)P_2 upon strong membrane depolarization (Murata et al., 2005). VSP, first discovered in ascidian *Ciona intestinalis* and later on in zebrafish (*Danio rerio* VSP [Dr-VSP]; Hossain et al., 2008), appeared as the first identified members of nonchannel proteins whose activity is regulated by membrane potential. This tool offers the possibility to trigger a rapid depletion of the PtdIns(4,5)P_2 pool in the plasma membrane. We thus aimed at testing the consequences of triggering the VSP enzymatic activity on E-C coupling. Results demonstrate that activation of the phosphatase depresses voltage-activated Ca^{2+} release, revealing a role for PtdIns(4,5)P_2 in the proper E-C coupling function.

MATERIALS AND METHODS

All experiments and procedures were performed in accordance with the guidelines of the local animal ethics committee of University Lyon 1, of the French Ministry of Agriculture (87/848), and of the European Community (86/609/EEC).

In vivo transfection

Expression was achieved by in vivo plasmid injection followed by electroporation, as described previously (Legrand et al., 2008; Weiss et al., 2010). Plasmids encoding the following proteins were used: Dr-VSP N-terminally tagged with EGFP, Dr-VSP and *C. intestinalis* VSP (Ci-VSP) in a bicistronic p-IRES-EGFP expression vector, and mRFP-tagged PLCδ_1PH domain (provided by T. Balla, National Institutes of Health, Bethesda, MD). In brief, 6–16-wk-old Swiss OF1 male mice were used. Transfection was performed in the flexor digitorum brevis (fdb) and interosseus muscles of the animals. Mice were anaesthetized by isoflurane inhalation using a commercial delivery system (Univentor 400 Anesthesia Unit; Univentor). 20 µl of a solution containing 2 mg/ml hyaluronidase dissolved in sterile saline was then injected into the footpads of each hind paw. 1 h later, the mouse was re-anaesthetized by isoflurane inhalation. A total volume of 20 µl of a solution containing 50 µg of plasmid DNA diluted in NaCl 9‰ was then injected into the footpads of the animal. After the injection, two gold-plated stainless steel acupuncture needles connected to the electroporation apparatus were inserted under the skin, near the proximal and distal portion of the foot, respectively. The standard protocol that we used consisted in 20 pulses of 200-V/cm amplitude and 20-ms duration delivered at a frequency of 2 Hz by a square wave pulse generator (BTX ECM 830; Harvard Apparatus). Muscle fiber isolation and experimental observations and measurements were performed 7–10 d later.

Preparation of isolated muscle fibers

Single fibers were isolated from the fdb and interosseus muscles from mice using a previously described procedure (Jacquemond, 1997). In brief, mice were killed by cervical dislocation before removal of the muscles. Muscles were treated with collagenase (type 1; Sigma-Aldrich) for 60 min at 37°C. Single fibers were then obtained by triturating the muscles within the experimental chamber. They were dispersed on the glass bottom of a 50-mm-wide culture µ-dish (Biovalley). For intracellular Ca^{2+} measurements under voltage-clamp conditions, fibers were first partially insulated with silicone grease so that only a 50–100-µm-long portion of the fiber extremity was left out of the silicone, as described previously (Jacquemond, 1997). The Ca^{2+}-sensitive fluorescent indicator rhod-2 was then introduced into the myoplasm by diffusion through the tip of the voltage-clamp pipette (see below). For all experimental situations, EGFP-negative (referred to as VSP-negative) fibers isolated from the same muscles were used as control. All experiments were performed at room temperature (20–22°C).

Electrophysiology

A patch-clamp amplifier (RK-400; Bio-Logic) was used in whole-cell voltage-clamp configuration. Command voltage-pulse generation was achieved with an analogue–digital converter (Digidata 1440A; Axon Instruments) controlled by pClamp 9 software (Axon Instruments). Fibers were bathed in the TEA-containing extracellular solution (see Solutions). Voltage clamp was performed with a micropipette filled with the rhod-2–containing intracellular-like solution (see Solutions). The tip of the micropipette was inserted through the silicone within the insulated part of the fiber and was crushed against the bottom of the chamber to ease intracellular equilibration. Analogue compensation was adjusted to further decrease the effective series resistance. Unless otherwise specified, membrane-depolarizing steps were applied from a holding command potential of −80 mV. For charge movement measurements, membrane current records were obtained in response to 100-ms-long depolarizing pulses of increasing amplitude from a holding potential of 0 mV. Removal of the linear leak and capacitive components of the current changes elicited by a depolarizing pulse was achieved using previously described procedures with record portions during pulses that were in some cases further corrected for sloping baseline (Collet et al., 2003; Pouvreau and Jacquemond 2005). Even with a depolarized holding potential, several fibers remained ineligible for charge movement analysis because of residual contaminating outward currents activated upon depolarization. When measuring Ca^{2+} transients in response to single depolarizing steps, a period of 30 s was allowed between two consecutive pulses. When the trains of 20 200-ms-long pulses (see Fig. 4) were applied, an interval of 1 min was allowed.

Confocal imaging

All experiments were conducted using a confocal microscope (LSM 5 Exciter; Carl Zeiss) equipped with a 63× oil-immersion objective (numerical aperture, 1.4). EGFP excitation was provided by the 488-nm line of an argon laser, and a 505-nm long-pass filter was used on the detection channel. For detection of either rhod-2 or PLCδ_1PH-mRFP fluorescence, excitation was

from the 543-nm line of a HeNe laser and fluorescence was collected above 560 nm. Intracellular Ca^{2+}-related rhod-2 fluorescence changes were imaged by using the line-scan mode (*x,t*) of the system with the line parallel to the longitudinal fiber axis. Images were taken with a scanning frequency of 1.15 ms per line. PLCδ$_1$PH-mRFP fluorescence was detected either in (*x,y*) or (*x,t*) mode. For measurements of the changes in transverse tubule membrane voltage upon voltage-clamp depolarization, muscle fibers were incubated for 30 min in the presence of 10 µM di-8-anepps before voltage clamp was achieved. Unless otherwise stated, di-8-anepps fluorescence was measured with the line-scan mode of the confocal microscope (1.93 or 1.15 ms per line) using the same configuration as for rhod-2 and mRFP, but with the pinhole fully open. Image processing and analysis was performed using ImageJ (National Institutes of Health) and Origin (OriginLab Corporation) software.

[Ca^{2+}] and Ca^{2+} release calculation

Rhod-2 fluorescence changes were expressed as F/F_0, where F_0 is the baseline fluorescence. No correction was made for the rhod-2–binding kinetics. Peak values for F/F_0 signals were measured as the first early peak of the transients. The Ca^{2+} release flux underlying the calculated global [Ca^{2+}] transients was estimated according to a previously described procedure (Collet et al., 2004; Pouvreau et al., 2006). Changes in [Ca^{2+}] were calculated from the rhod-2 signals using the previously described pseudo-ratio equation (Cheng et al., 1993) assuming a basal [Ca^{2+}] of 100 nM and a K_d of rhod-2 for Ca^{2+} of 1.2 µM. SR calcium release flux was then calculated from the time derivative of the total myoplasmic Ca^{2+} ($[Ca]_{Tot}$) obtained from the occupancy of intracellular calcium-binding sites. The model included troponin C–binding sites, parvalbumin-binding sites, and calcium transport across the SR membrane with the same parameters as used in Lefebvre et al. (2011, 2013). Ca^{2+}-binding sites on EGTA were included with a total site concentration of 6 mM, an "on" rate constant $k_{on,EGTA}$ of 0.056 $\mu M^{-1} \cdot ms^{-1}$ and an "off" rate constant $k_{off,EGTA}$ of 0.002 ms^{-1}.

Solutions

The extracellular solution used for whole-cell voltage clamp contained (mM): 140 TEA-methanesulfonate, 2.5 $CaCl_2$, 2 $MgCl_2$, 1 4-aminopyridine, 10 HEPES, and 0.002 tetrodotoxin. The intracellular-like solution for whole-cell voltage clamp contained (mM): 120 K-glutamate, 5 Na_2-ATP, 5 Na_2-phosphocreatine, 5.5 $MgCl_2$, 10 EGTA, 4 $CaCl_2$, 5 glucose, and 5 HEPES. All solutions were adjusted to pH 7.20.

Statistics

Least-squares fits were performed using a Marquardt–Levenberg algorithm routine included in Origin (OriginLab Corporation). Data values are presented as means ± SEM for *n* fibers. Statistical significance was determined using a Student's *t* test (*, $P \leq 0.05$).

Online supplemental material

Fig. S1 shows results from measurements of intramembrane charge movement in VSP-negative and VSP-positive fibers. Fig. S2 presents results from measurements of changes in transverse tubule membrane voltage using the dye di-8-anepps. Fig. S3 shows the voltage-dependent properties of the DHPR Ca^{2+} current in VSP-negative and VSP-positive fibers. Results from measurements of intramembrane charge movement, of di-8-anepps fluorescence, and of DHPR Ca^{2+} current are described in detail in the text accompanying Figs. S1, S2, and S3, respectively. Videos 1 and 2 show a sequence of confocal images of PLCδ$_1$PH-mRFP fluorescence from two fibers also expressing Ci-VSP and depolarized by 5-s-long pulses. The online supplemental material is available at http://www.jgp.org/cgi/content/full/jgp.201411309/DC1.

RESULTS

Functional expression of Ci-VSP and Dr-VSP in mouse muscle fibers

Ci-VSP and Dr-VSP exhibit distinct voltage sensitivity and speed of activation, and their robustness of expression also appears to differ in cultured mammalian cells (Hossain et al., 2008). As these differences were expected to also occur in our system and to make one or the other more efficient in depleting plasma membrane PtdIns(4,5)P_2, it was of specific interest to test their respective effect. Fig. 1 A shows a transmitted light image and corresponding confocal image of a portion of a muscle fiber transfected with Ci-VSP using the pIRES-EGFP plasmid. Fig. 1 B shows an analogous pair of images from a fiber expressing Dr-VSP N-terminally tagged with EGFP (EGFP–Dr-VSP). In all cases, expression of VSP proteins was well tolerated: there was no apparent consequence on fiber appearance and morphology. There was also no sign of alterations such as blebbing and membrane extensions, which might have been expected because phosphoinositides are involved in regulation of cell morphology and cytoskeleton (see, for instance, Yamaguchi et al., 2014). For the batches of VSP-negative and Ci-VSP–positive

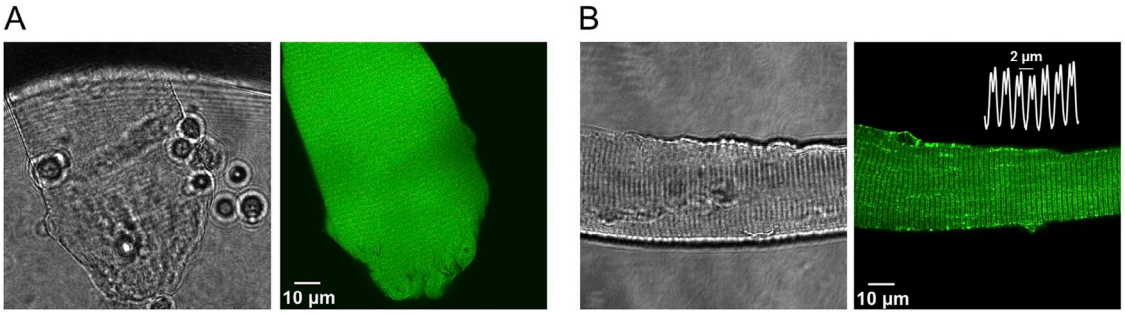

Figure 1. Expression of VSP in muscle fibers. Transmitted light images and corresponding confocal images of a portion of muscle fibers expressing Ci-VSP using the pIRES-EGFP plasmid (A) and Dr-VSP N-terminally tagged with EGFP (B). In B, the white trace superimposed on the green image shows the typical banded pattern of the fluorescence along the longitudinal axis of the fiber.

fibers used in Fig. 4, mean fiber diameter was 51.5 ± 2.8 µm (n = 17) and 49.5 ± 2.0 µm (n = 17), respectively; corresponding mean measured capacitance was 1,599 ± 120 pF (n = 21) and 1,544 ± 210 pF (n = 19), which, considering that a similar length of fiber was always under voltage clamp, indicates that there was no significant difference in transverse tubule density between VSP-negative and Ci-VSP–positive fibers.

Although expression of EGFP with the pIRES plasmid produced an expected homogenous fluorescence, expression of the EGFP–Dr-VSP fusion protein revealed a clear double-striped transverse pattern with an ~2-µm spacing interval, reminiscent of the triadic area. This pattern does not disclose which membrane compartment of the triad is targeted by the VSP. However, considering that previous works in various expression systems established that VSPs localize in the plasma membrane, it is very likely that under our conditions, the striated pattern corresponded to the transverse tubule membrane system of the muscle fibers.

With the aim of formally establishing the VSP protein localization in the transverse tubule membrane, we attempted to measure intramembrane charge movement in VSP-negative and VSP-positive fibers maintained at a holding voltage of 0 mV. These measurements could not be made entirely acceptable because several fibers were not suitable for analysis as a result of remaining voltage-activated contaminating outward currents. Furthermore, a transient inward current component at the onset of the depolarizing pulses complicated the analysis. For these

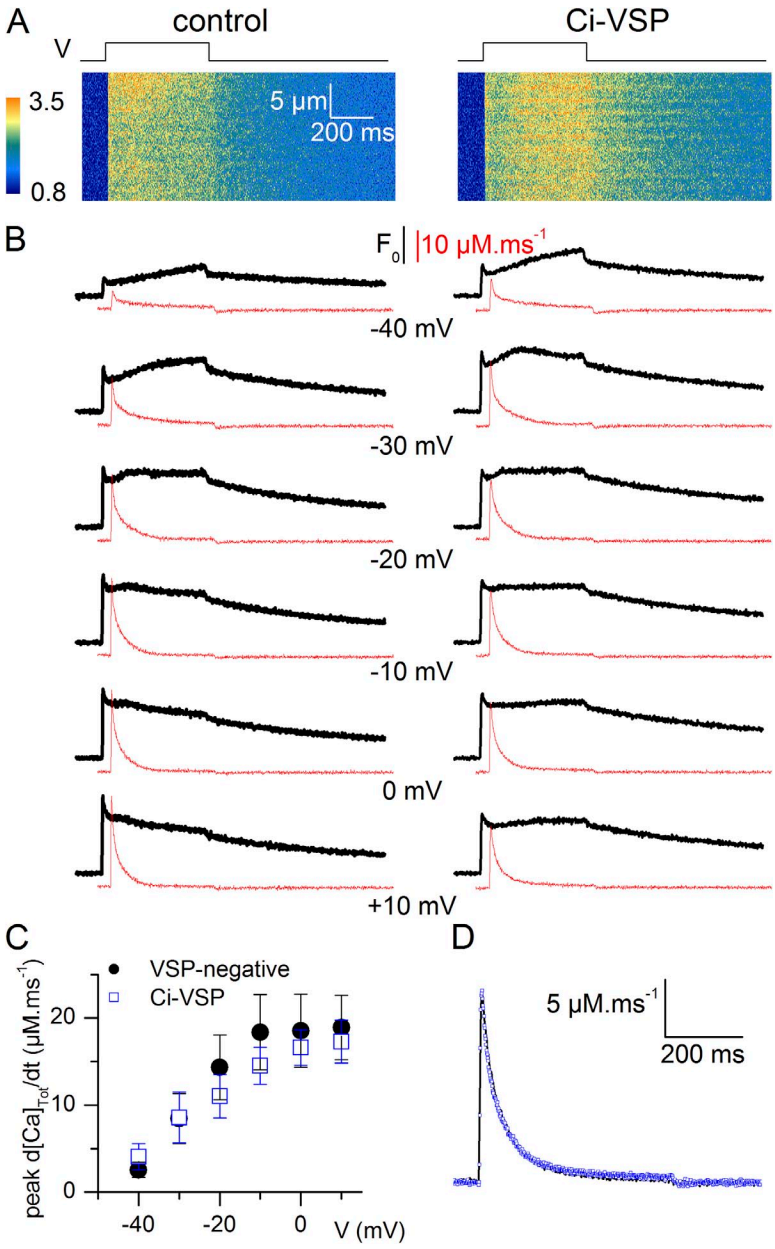

Figure 2. Voltage-activated Ca^{2+} release in VSP-expressing fibers. (A) Line-scan images of depolarization-induced Ca^{2+} release in a VSP-negative fiber (left) and in a Ci-VSP–expressing fiber (right); fibers were depolarized from −80 to 10 mV (traces on top). (B) Ca^{2+} transients (rhod-2 F/F_0, thick traces) and corresponding rate of Ca^{2+} release (thin red traces) in response to pulses from −80 mV to the indicated values. (C) Peak Ca^{2+} release versus voltage in VSP-negative fibers (n = 9) and in Ci-VSP–expressing fibers (n = 6). Error bars represent ± SEM. (D) Average Ca^{2+} release in response to a pulse from −80 to 10 mV in VSP-negative fibers (line) and in Ci-VSP–expressing fibers (blue squares).

reasons, we present and discuss corresponding results in the supplemental text. Despite these difficulties, results shown in Fig. S1 indicate that membrane current components yielding properties consistent with those of gating currents of VSP proteins are detectable in the transfected fibers, supporting the presence of VSPs in the transverse tubule membrane. Thus, the present system is effective to assess the consequences of their activation on Ca^{2+} homeostasis and E-C coupling.

Ca^{2+} release in response to single depolarizing steps in VSP-expressing fibers

SR Ca^{2+} release is physiologically activated within a range of membrane voltages that is more negative than the one needed to activate Ci-VSP or Dr-VSP. Our main goal was to take advantage of this shift to compare the properties of Ca^{2+} transients elicited by voltage pulses that would maximally activate Ca^{2+} release with or without activating the VSP. We first tested whether presence of the VSP proteins per se in the transverse tubule membrane affects the properties of Ca^{2+} release independently from the phosphatase activity. Fig. 2 A shows illustrative examples of line-scan confocal images of rhod-2 fluorescence taken from a VSP-negative fiber (left) and from a fiber expressing Ci-VSP (right). Both fibers were step-depolarized by a 0.5-s-long depolarization from −80 to 10 mV. Fig. 2 B shows the time course of change in rhod-2 fluorescence (thick traces) and the corresponding calculated rate of release (thin traces) in response to 0.5-s-long pulses of increasing amplitude, in these two fibers. Expression of Ci-VSP had no striking consequence on the Ca^{2+} signals: in both fibers, Ca^{2+} release was activated at a similar threshold voltage level and yielded the classical waveform characterized by an early peak that rapidly decayed toward a lower level. Fig. 2 C presents mean values for peak Ca^{2+} release versus voltage in VSP-negative fibers ($n = 9$) and in Ci-VSP–expressing fibers ($n = 6$): there was no statistical difference between the values in the two groups. The same measurements performed in three fibers expressing Dr-VSP gave mean values in the same range (not depicted). Fig. 2 D shows the average Ca^{2+} release trace in response to a 0.5-s-long pulse to 10 mV in VSP-negative fibers and in Ci-VSP–expressing fibers. There was no sign of any difference in the time course of Ca^{2+} release in the VSP-expressing fibers.

According to previous works, substantial depletion of plasma membrane PtdIns(4,5)P_2 requires at least several hundred milliseconds of VSP activation by a strong membrane depolarization, whereas subsequent recovery from depletion occurs over a time scale of seconds to tens of seconds (see, for instance, Sakata et al., 2011). Because upon membrane depolarization SR Ca^{2+} release exhibits an early peak that falls within 10–20 ms toward a low, slowly declining level, we did not expect a sustained strong depolarization to be the optimal protocol to reveal a potential effect of VSP activation, as PtdIns(4,5)P_2 would become substantially depleted at a time when Ca^{2+} release is very low. Furthermore, such long pulses cannot

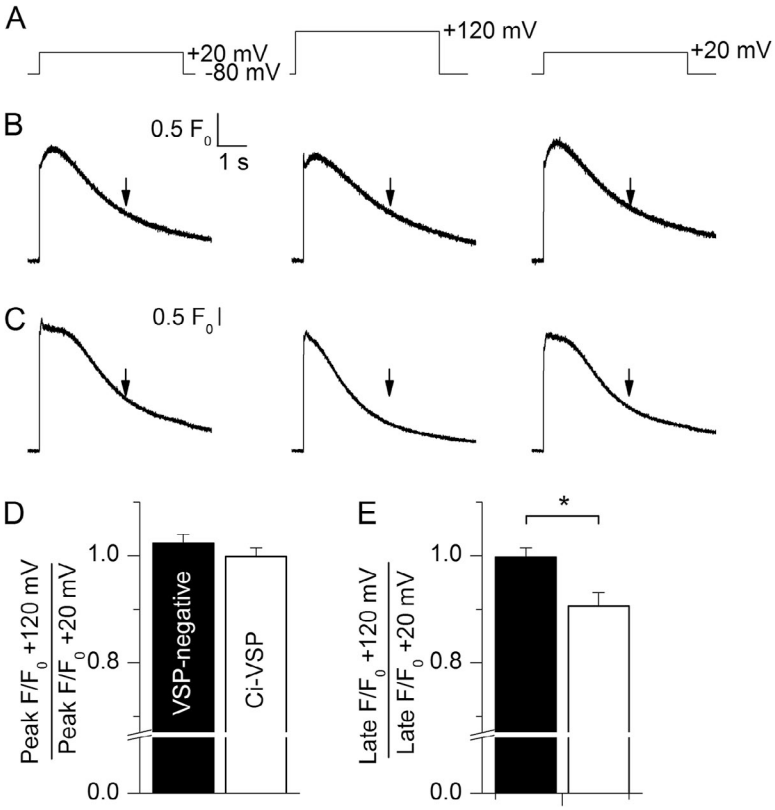

Figure 3. Ca^{2+} transients in VSP-expressing fibers depolarized by large pulses. (A) Voltage-pulse protocol. (B and C) Corresponding F/F_0 rhod-2 traces in a Ci-VSP–negative and in a Ci-VSP–positive fiber, respectively. Arrows point to the F/F_0 level 3 s after the onset of the pulse. (D) Mean values for the ratio of the initial peak rhod-2 Ca^{2+} transient in response to the pulse to 120 mV to the initial peak value in response to the pulse to 20 mV in VSP-negative ($n = 11$) and Ci-VSP–positive fibers ($n = 8$). (E) Mean values for the ratio of the rhod-2 Ca^{2+} level 3 s after the onset of the pulse to 120 mV to the corresponding value during the pulse to 20 mV. Error bars represent ± SEM. *, $P \leq 0.05$.

be repeated at a frequency that would seem sufficiently high to avoid PtdIns(4,5)P_2 repletion between pulses, as the time for recovery of Ca^{2+} release from SR Ca^{2+} depletion, and also to some extent from voltage-dependent inactivation, precludes repeating such pulses with a short interval. We nevertheless did compare Ca^{2+} transients triggered by 5-s-long depolarizing pulses to 20 mV (non-VSP–activating pulse) and to 120 mV (VSP-activating pulse) in VSP-negative and VSP-positive fibers. Fig. 3 (B and C) shows rhod-2 fluorescence transients elicited by stepping the membrane potential from −80 to 20 mV, then from −80 to 120 mV, and then again from −80 to 20 mV in a Ci-VSP–negative fiber and in a Ci-VSP–positive fiber, respectively. The three fluorescence transients looked quite similar in the VSP-negative fiber, but in the VSP-expressing fiber, the fluorescence signal appeared to be less sustained late during the pulse to 120 mV as compared with the level during the bracketing pulses to 20 mV. Fig. 3 (D and E) shows mean values for the ratio of the initial peak and of the late (3 s after the beginning of the pulse) rhod-2 Ca^{2+} transients in response to the pulse to 120 mV versus corresponding values in response to the pulses to 20 mV in VSP-negative (n = 11) and Ci-VSP–positive fibers (n = 8). In each fiber, initial and late F/F_0 values for the pulse to 120 mV were divided by the average of the two respectively corresponding bracketing values measured in response to the pulses to 20 mV. The mean ratio for initial peak Ca^{2+} transient did not statistically differ between the two groups of fibers. In contrast, the mean ratio for the Ca^{2+} level 3 s after the beginning of the pulse was significantly depressed in Ci-VSP–expressing fibers as compared with the mean value in VSP-negative fibers (P = 0.007).

The strong depolarizing pulses used to activate the VSP inevitably triggered substantial activation of outward K^+ current, which was expected to affect the quality of the

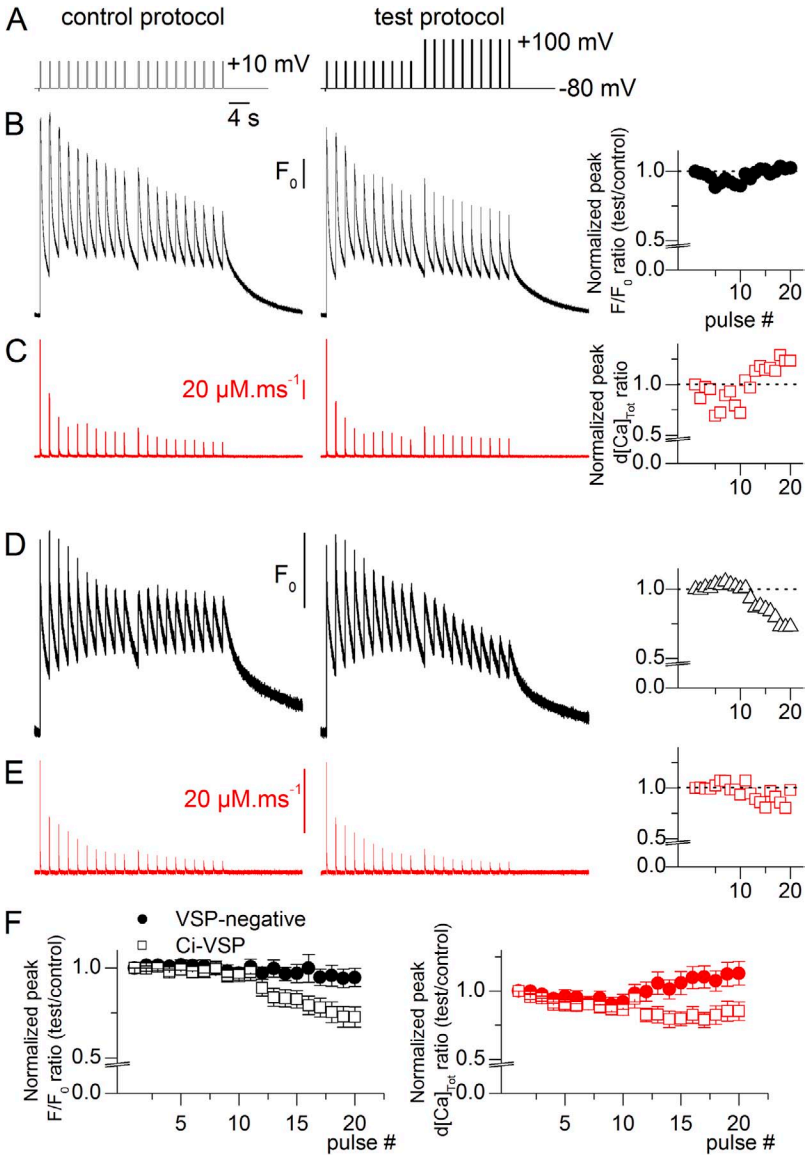

Figure 4. Ca^{2+} transients in response to trains of depolarizing steps in VSP-negative fibers and Ci-VSP–expressing fibers. (A) Control and test voltage-pulse protocols. (B and D) Rhod-2 F/F_0 traces recorded in response to the protocols shown in A in a VSP-negative fiber and in a Ci-VSP–expressing fiber, respectively. The graphs on the right show the ratio of the successive peak F/F_0 values during the test record to the corresponding values during the control record, plotted versus the pulse number during the protocols; values were normalized to the ratio value corresponding to the first Ca^{2+} transient. (C and E) Ca^{2+} release traces calculated from the above-corresponding rhod-2 transients. The graphs on the right show the ratio of the successive peak Ca^{2+} release values during the test record to the corresponding values during the control record, plotted versus the pulse number; values were normalized to the ratio value corresponding to the first Ca^{2+} transient. (F; left) Mean values for the normalized ratio of peak F/F_0 during the test record to the corresponding peak F/F_0 during the control record, versus the pulse number, in VSP-negative and in Ci-VSP–positive fibers. (Right) Corresponding mean values for the normalized ratio of peak Ca^{2+} release during the test record to the corresponding peak Ca^{2+} release during the control record. Error bars represent ± SEM.

voltage control. To estimate the actual voltage reached in the transverse tubule membrane of the voltage-clamped portion of fiber during these pulses, we measured the changes in fluorescence of the voltage-sensitive dye di-8-anepps in nontransfected muscle fibers. Results from these measurements are presented in Fig. S2. They suggest that during command pulses to 100 or 120 mV, the actual transverse tubule voltage reached ~60 mV, sufficient to substantially activate Ci-VSP.

Ca^{2+} release in response to trains of depolarizing steps in Ci-VSP–expressing fibers

To maximize the likelihood of severely depleting PtdIns(4,5)P_2 through VSP activation while maintaining the potency to trigger substantial Ca^{2+} release, we used a protocol consisting in successive 200-ms-long depolarizing pulses applied every 2 s. Although under such conditions peak Ca^{2+} release decreased over time as pulses were applied, a significant activity could be maintained over a period of ~1 min (Fig. 4). Fig. 4 A shows the exact protocol used in each fiber: a 200-ms-long pulse was applied 10 times from −80 to 10 mV and then 10 times again to either 10 mV (control protocol) or to 100 mV (test, VSP-activating, protocol). The 10 first Ca^{2+} transients were used to assess the reproducibility of the changes in Ca^{2+} in the test versus the control record in response to the same pulses that did not activate the VSP. The next 10 pulses were anticipated to reveal the effect of VSP activation in the test record. B and D in Fig. 4 show such pairs of records from a VSP-negative fiber and from a Ci-VSP–expressing fiber, respectively. In both fibers, as the successive pulses were applied, Ca^{2+} transients were triggered and decayed to an elevated level. In the VSP-negative fiber, the two records looked quite similar. In contrast, in the Ci-VSP–expressing fiber, there was a progressive drop in the amplitude of the Ca^{2+} transients as pulses to 100 mV were applied. Independent of the presence of VSP, there was fiber to fiber variability in the overall time course of change in peak and baseline Ca^{2+} levels along the records. For instance, the fact that the peak rhod-2 transient appeared more sustained along the last 10 pulses in Fig. 4 D as compared with Fig. 4 B was absolutely not a reproducible feature of the VSP-expressing fiber (see, for instance, Fig. 6). Furthermore, in a given fiber the actual amplitude of peak Ca^{2+} transients in response to the first 10 pulses also could somewhat vary between the control and the test record. For analysis, successive peak F/F_0 values during the test record were thus divided by the corresponding values in the control record; values for this ratio were then normalized to the ratio value corresponding to the first Ca^{2+} transient of the train. The right-end graph in Fig. 4 (B and D) shows values for the ratio plotted versus the pulse number for the two fibers. Corresponding mean values from 21 VSP-negative fibers and 19 Ci-VSP–expressing fibers are reported in the left panel of Fig. 4 F. Although in the VSP-negative fibers the ratio remained close to unity for all Ca^{2+} transients, there was a clear drop in the ratio as pulses to 100 mV were applied in the Ci-VSP–expressing fibers. Statistical comparison of the values revealed a significant difference between VSP-negative and Ci-VSP–expressing fibers, starting from pulse number 13 (third pulse to 100 mV). For instance, the mean ratio value corresponding to the last pulse in the protocols was 0.73 ± 0.06 and 0.95 ± 0.05 for Ci-VSP–positive fibers and VSP-negative fibers, respectively ($P = 0.006$). Statistical difference was also tested versus the hypothesis of the ratio being 1. For the VSP-negative fibers, none of the mean ratio values significantly differed from 1, whereas for the Ci-VSP fibers, all ratio values starting from pulse number 12 were significantly lower than 1.

A similar analysis was performed from the peak values of the Ca^{2+} release flux calculated from the rhod-2 traces. Flux traces corresponding to the rhod-2 signals from the VSP-negative and VSP-expressing fibers illustrated in Fig. 4 are shown in C and E, with the right-side graph showing values for the test over control ratio plotted versus the pulse number. Corresponding mean values are reported in the right panel in Fig. 4 F. Mean values from the VSP-expressing fibers were significantly depressed as compared with values in VSP-negative fibers starting from pulse number 13.

We asked whether the presence and/or activation of VSP had consequences on the membrane current flowing during the pulses. We measured membrane current near the end of each depolarizing pulse applied during

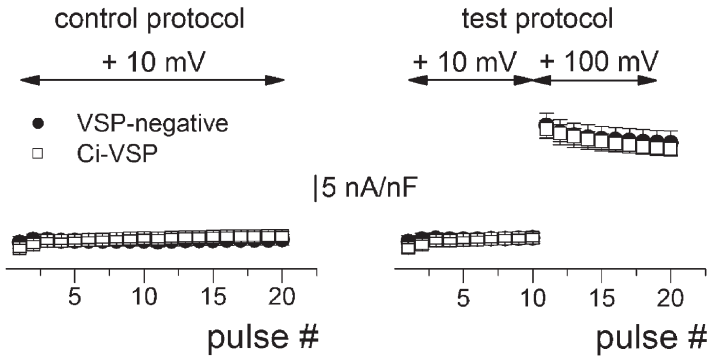

Figure 5. Membrane current during trains of depolarizing steps in VSP-negative fibers and Ci-VSP–expressing fibers. Mean value for the membrane current measured at the end of each depolarizing pulse during the control and test protocols shown in Fig. 4. The horizontal axis is positioned at the zero-current level. Error bars represent ± SEM.

the control and test protocol, and values were normalized to fiber capacitance. Corresponding mean values are presented in Fig. 5. There was no indication that either the presence of Ci-VSP in the membrane or its activation by the pulses to 100 mV produced any modification of the membrane current.

To test whether the depressing effect of Ci-VSP activation on Ca^{2+} release was reversible and repeatable, two test protocols were applied, bracketed by control protocols, in a subset of fibers. This appeared to be the case, as Fig. 6 illustrates. Fig. 6 B shows F/F_0 rhod-2 traces elicited in a Ci-VSP–expressing fiber alternatively challenged by a control and a test protocol (Fig. 6 A). Fig. 6 C shows mean values for the peak F/F_0 values during the test 1, control 2, and test 2 records, all divided by the corresponding values in the control 1 record. Values are from 12 Ci-VSP–expressing fibers. The drop in Ca^{2+} release elicited by the first set of pulses to 100 mV was transient and could be triggered again by a second series of the same pulses, consistent with reversible reduction in the level of a molecule with agonistic properties toward Ca^{2+} release.

Ca^{2+} release in response to trains of depolarizing steps in Dr-VSP–expressing fibers

The 200-ms pulse-train control and test protocols described above were also tested in fibers expressing Dr-VSP, a teleost orthologue of VSP, which exhibits a more positive voltage dependence than Ci-VSP. As illustrated in Fig. 7 (B and C), Dr-VSP–expressing fibers responded in a similar manner to Ci-VSP–expressing fibers. However, out of seven fibers tested, two did not respond with any drop at all in the ratio (of peak F/F_0 values during the test record to corresponding values in the control record) when the pulses to 100 mV were applied. As a consequence, none of the mean ratio values significantly differed from the corresponding ones in the VSP-negative fibers. Still, when testing the mean values versus the hypothesis of the ratio being 1, values for pulses number 15 and above were significantly depressed. Dr-VSP appeared thus less efficient than Ci-VSP in depressing Ca^{2+} release, but this was expected because it requires more positive voltage steps to be activated.

Ca^{2+} current after strong depolarizing pulses in Ci-VSP–expressing fibers

The above data are consistent with the possibility that activation of VSP in the transverse tubule membrane affects Ca^{2+} release. We examined whether the function of Cav1.1, which acts both as voltage sensor for E-C coupling and as voltage-dependent Ca^{2+} channel, would be affected after VSP activation. For this, we measured the Ca^{2+} current in fibers challenged by a double-pulse protocol. The membrane voltage was first stepped from −80 to 20 mV for 5 s (prepulse) and then, after a 1-s delay, from −80 to 20 mV for 1 s (test pulse). The double pulse was then applied with the prepulse to 120 mV to activate the VSP and then again with the prepulse to 20 mV as a bracketing control. In each fiber, the whole protocol was repeated with a 2-s and with a 5-s interval between the prepulse and the test pulse. Corresponding membrane current traces from a Ci-VSP–expressing fiber are shown in Fig. 8 (A–C). In each panel, the two membrane current records with the prepulse to 20 mV are in black, and the record with the prepulse to 120 mV is in red.

Ci-VSP expression per se did not affect the amplitude of the Ca^{2+} current: the mean peak value of the current

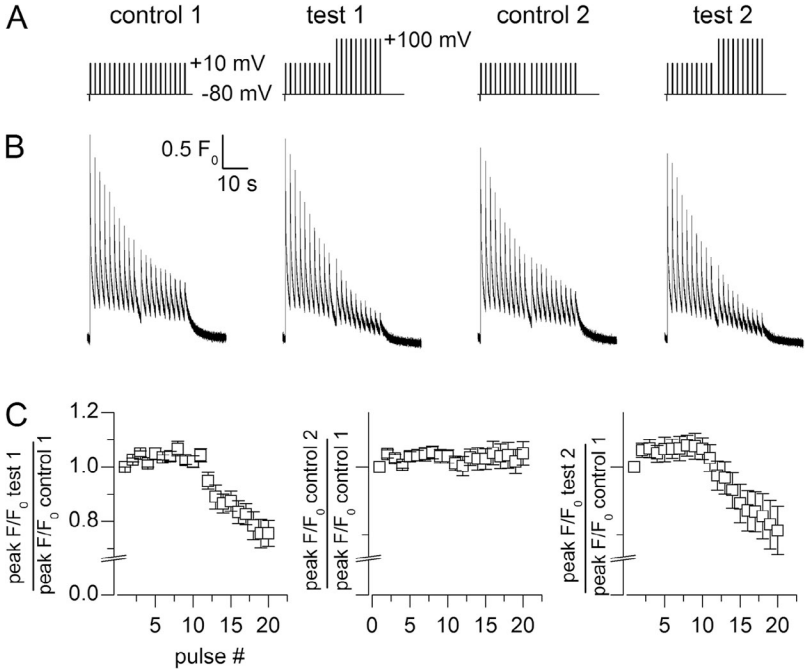

Figure 6. Reversibility of the effect of VSP activation on trains of Ca^{2+} transients. (A) Pulse protocols that were successively applied. (B) F/F_0 rhod-2 traces elicited in a Ci-VSP–expressing fiber challenged by the protocols shown in A. (C) Mean values for the peak F/F_0 rhod-2 signals during the test 1, control 2, and test 2 records (n = 12 Ci-VSP–expressing fibers); in each fiber, successive peak F/F_0 values were divided by the corresponding values for the same pulse number during the control 1 record. Error bars represent ± SEM.

during the 5-s-long prepulse to 20 mV was −2.5 ± 0.6 A/F and −3.3 ± 0.6 A/F in VSP-negative (n = 7) and VSP-positive fibers (n = 8), respectively, not significantly different. The peak amplitude of the calcium current during the test pulse was depressed as compared with its amplitude during the prepulse to 20 mV, as expected from only partial recovery from voltage-dependent inactivation. Interestingly, the prepulse to 120 mV actually seemed to slightly enhance the Ca^{2+} current amplitude during the test pulse as compared with the prepulse to 20 mV, an effect that was observed in both VSP-negative and VSP-positive fibers. Reasons for this effect are currently being explored, independent from the present work. In any case, we found no indication that activation of the VSP had an effect on the Ca^{2+} channel activity. Fig. 8 D shows mean values for the ratio of the Ca^{2+} current amplitude after the prepulse to 120 mV to its amplitude after the prepulse to 20 mV (average of the two bracketing values) versus the pulse interval. Membrane current amplitudes were measured as the difference between the peak and the end-pulse level. There was no statistical difference between mean ratio values in VSP-negative and VSP-positive fibers. Although one cannot exclude that even the shortest interval at −80 mV (1 s) could allow some recovery from the consequences of the phosphatase activity, results provide no indication that Cav1.1 Ca^{2+} current amplitude is a sensitive target of this activity. In a separate series of experiments, we compared the voltage dependence of the Ca^{2+} current properties between VSP-negative and VSP-positive fibers (Fig. S3). Results provided again no indication that the peak amplitude and also the time to peak of the current would differ between VSP-negative fibers and Ci-VSP– and Dr-VSP–expressing fibers. Regarding the mean values for the time constant of current decay, they did not significantly differ between VSP-negative fibers and either Ci-VSP– or Dr-VSP–expressing fibers. Values were, however, significantly larger in Ci-VSP–expressing fibers than in Dr-VSP–expressing fibers at 20 (P = 0.039), 30 (P = 0.009), and 40 mV (P = 0.003). Because Ci-VSP would be activated to some extent at these voltages, this may be an indication that Ca^{2+} current inactivation is sensitive to the consequences of the phosphatase activity.

PtdIns(4,5)P_2 level after depolarization of Ci-VSP–expressing fibers

To explicitly assess in our conditions the ability of VSP activation to deprive plasma membrane PtdIns(4,5)P_2, we coexpressed Ci-VSP (using the pIRES-EGFP plasmid) together with the PtdIns(4,5)P_2-selective PLCδ_1-PH domain (Stauffer et al., 1998; Várnai and Balla, 1998) tagged with mRFP, and we followed the corresponding changes in fluorescence upon membrane depolarization. For simplicity, we will refer to PLCδ_1PH-mRFP fluorescence as "mRFP fluorescence." Fig. 9 A shows confocal images of GFP and of mRFP fluorescence from such a cotransfected muscle fiber. The enlarged view of the mRFP fluorescence on the right, together with the graph below which is reporting the fluorescence intensity along a rectangular region of interest, clearly shows that mRFP yielded a characteristic triadic pattern, namely double-banded transverse-oriented striations spaced by ∼2 µm. The closed circles in Fig. 9 B show the time course of change in mRFP fluorescence averaged over an entire given area of the fiber while applying 5-s-long depolarizing pulses according to the protocol shown on top; for this, a confocal x,y image was taken every 1.97 s. The sequence of images at lower resolution is presented as Video 1. The open circles in Fig. 9 B show the time course of change in mRFP fluorescence measured afterward,

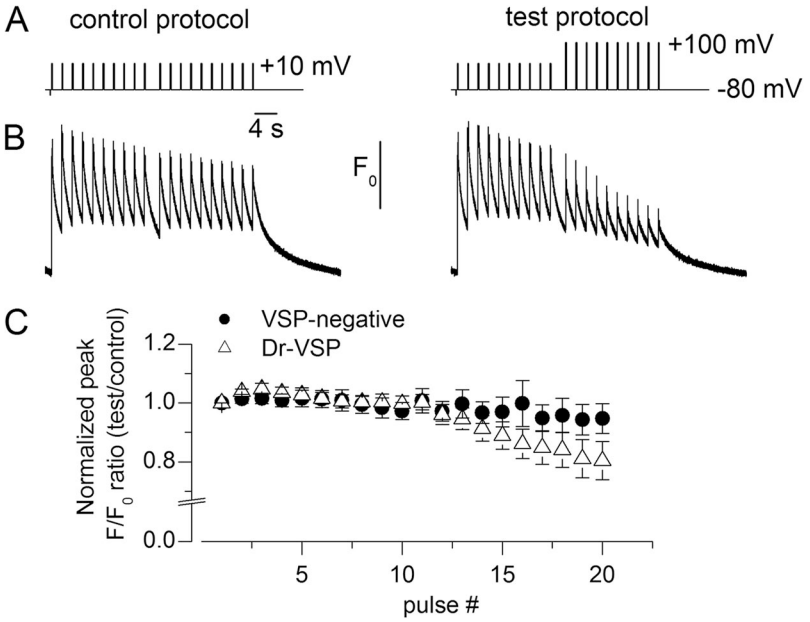

Figure 7. Ca^{2+} transients in response to trains of depolarizing steps in Dr-VSP–expressing fibers. (A) Control and test voltage-pulse protocols. (B) Rhod-2 F/F_0 traces recorded in response to the protocols shown in A in a Dr-VSP–positive fiber. (C) Mean values for the normalized ratio of peak F/F_0 during the test record to the corresponding peak F/F_0 during the control record, versus the pulse number in Dr-VSP–positive fibers (n = 7). Mean values for VSP-negative fibers are the same as in Fig. 4. Error bars represent ± SEM.

over a nearby fiber area, while no pulse was applied. Although we tried to keep laser excitation as low as possible, there was quite substantial mRFP photobleaching over time. Nevertheless, on top of photobleaching, clear positive changes in fluorescence were triggered by the largest depolarizing pulses. In Fig. 9 C, the time course of change in fluorescence associated with the depolarizing pulse protocol was corrected for photobleaching. To do so, values were divided by the time-corresponding ones in the subsequent record taken when no pulse was applied (closed circles in Fig. 9 C). As an alternative, a two-exponential function was fitted to the time course of baseline decay in fluorescence in the series of measurements taken while the voltage steps were applied; for this, only the 20 first and 20 last values in the trial were used for the fit. From this, a synthetic series of decaying values was generated (superimposed line plot in Fig. 9 B), which was then used to normalize fluorescence values associated with the depolarizing pulses. The result from this correction is shown as open circles in Fig. 9 C. The two correction procedures provided a very similar result: there was a clear transient rise in mRFP fluorescence in response to the pulses to 50, 90, and 110 mV. Identical measurements performed in three fibers isolated from a muscle expressing only the PLCδ_1-PH domain and not the VSP showed absolutely no change in fluorescence upon membrane depolarization (not depicted).

A quantitative estimate of the kinetics of the depolarization-induced changes in mRFP fluorescence was made by fitting a single-exponential function to the time course of fluorescence increase upon membrane depolarization and of fluorescence recovery after membrane repolarization, when this could be reliably performed. This was intended to only provide an order of magnitude of the rate of changes, as photobleaching correction could not be perfectly accurate and corrupted to some extent the kinetics of voltage-induced mRFP changes. The time constant of rise estimated from data collected from four

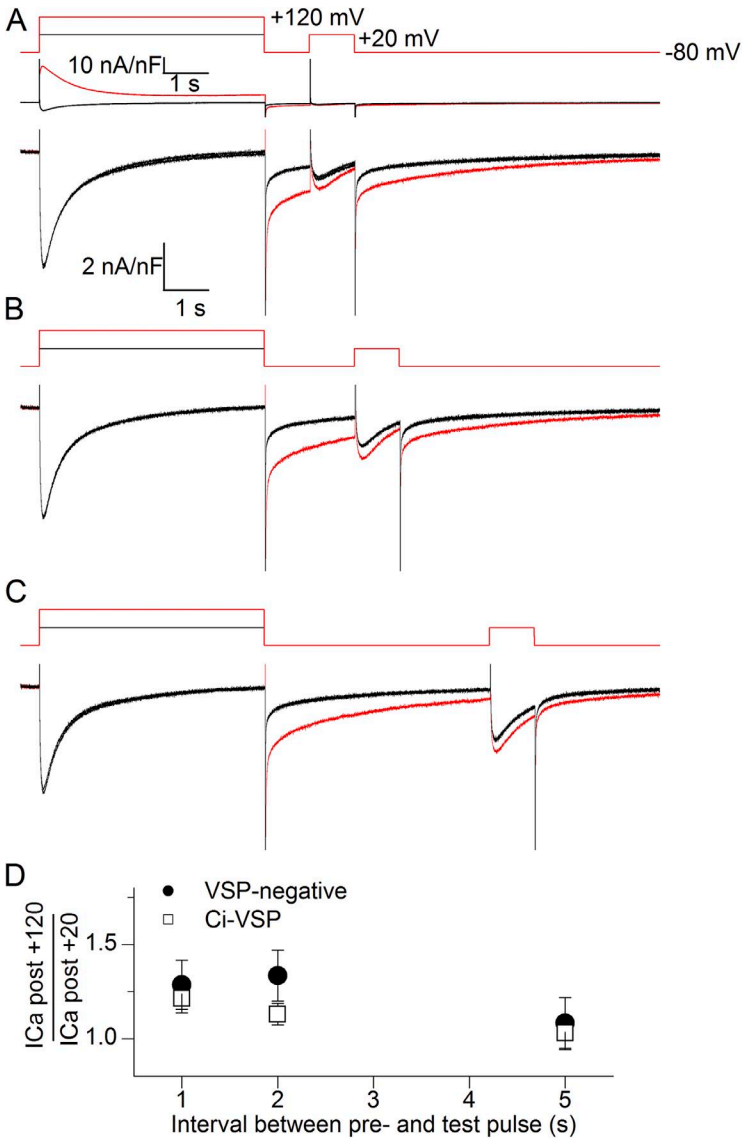

Figure 8. Ca^{2+} current after strong depolarizing pulses in Ci-VSP–expressing fibers. In each panel, top traces show the two voltage-pulse protocols that were applied to the fiber; the protocol with prepulse to 120 mV (test) was bracketed by two protocols with prepulse to 20 mV (controls). (A–C) Superimposed membrane current records in response to the above shown protocols. Currents recorded during the two control protocols are in black, whereas current elicited by the test protocol is presented in red. In A, records are presented at both low (top) and high magnification (bottom). In B and C, only the high magnification views are presented. (D) Mean values for the ratio of Ca^{2+} current amplitude after the prepulse to 120 mV to its amplitude after the prepulse to 20 mV; values are plotted versus the pulse interval between the pre- and test pulses. Results are from seven VSP-negative and eight Ci-VSP–positive fibers. Error bars represent ± SEM.

fibers challenged with a 20-s-long depolarizing pulse to 40 or 50 mV and to 100 or 110 mV was 14.8 ± 4 s and 7.5 ± 2 s, respectively. The time constant of mRFP fluorescence recovery after membrane repolarization was 14.3 ± 4.5 s after a pulse to 40 or 50 mV ($n = 5$) and 13.9 ± 3 s after a pulse to 90–110 mV ($n = 6$), respectively. The fact that the rate of rise increased with the amplitude of the depolarizing pulse further supports the conclusion that this signal results from voltage-evoked VSP enzyme activity. It is also worth noting that the rate of rise of the mRFP signal upon strong depolarization is much slower than the kinetics of Ca^{2+} release. This confirms our postulate (in relation with Fig. 3) that during a sustained depolarization, PtdIns(4,5)P_2 becomes substantially depleted at a time when Ca^{2+} release is very low.

Spatially segregated distinct changes in PtdIns(4,5)P_2 after Ci-VSP activation

Careful viewing of Video 1 reveals that the striated pattern of mRFP fluorescence tends to vanish during the strong depolarizing pulses. This effect of membrane depolarization upon the spatial distribution of mRFP fluorescence is examined in Fig. 10. Fig. 10 A shows three confocal images of mRFP fluorescence taken from another fiber before, during, and after a 5-s-long pulse to 50 mV. The corresponding whole sequence of successive images is presented as Video 2. The graph below each image in Fig. 10 A shows the fluorescence intensity profile along the highlighted rectangular area (Fig. 10 A, left). During the depolarizing pulse, the average fluorescence was slightly increased, accompanied by a clear attenuation of the transverse triadic profile, a phenomenon that was reversible after membrane repolarization. The fluorescence intensity at a given location of the profile during the pulse (Fluo+50) was subtracted from its corresponding initial/resting intensity before the pulse (Fluo−80(1)), and the difference is plotted versus the initial fluorescence intensity (Fluo−80(1)) in the left panel of Fig. 10 B. The result shows a clear negative slope with the difference being positive for the lowest levels of initial/resting fluorescence intensity and negative for the largest. According to the standard interpretation of the banded intensity profile, within the limits of the confocal resolution (with respect to triadic membrane compartment versus cytosolic volume), lowest values of initial/resting fluorescence are likely to report a

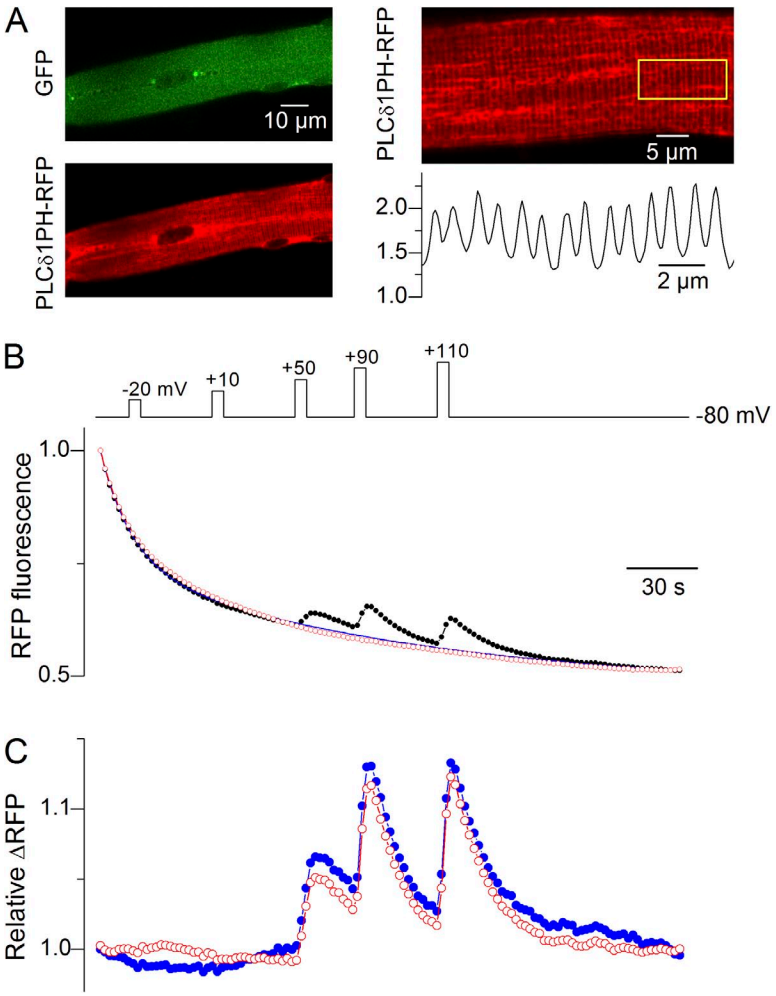

Figure 9. PLCδ_1PH-mRFP fluorescence in fibers expressing Ci-VSP. (A) Confocal images of a portion of a muscle fiber expressing Ci-VSP using the pIRES-EGFP plasmid and PLCδ_1PH-mRFP. The image on the right shows the PLCδ_1PH-mRFP fluorescence at higher magnification, and the graph below shows the fluorescence profile along the longitudinal axis of the highlighted rectangular region (yellow box). (B) Time course of change in PLCδ_1PH-mRFP fluorescence averaged over a given area of the fiber while applying 5-s-long depolarizing pulses according to the protocol shown on top (closed circles); superimposed time course of change in PLCδ_1PH-mRFP fluorescence measured subsequently over a nearby fiber area while no pulse was applied (open circles); synthetic trace generated from a two-exponential fit to the closed-circles record, using only the 20 first and 20 last values in the record for the fit (line). (C) Changes in fluorescence associated with the depolarizing pulse protocol after normalization by the record taken when no pulse was applied (closed circles); changes in fluorescence associated with the depolarizing-pulse protocol after normalization by the synthetic record (open circles).

dominant cytosolic contribution, whereas highest values should encompass a more important triadic membrane contribution, which we will assume here to correspond to the transverse tubule. Accordingly, the depolarizing pulse induces a depression of transverse tubule–bound mRFP and an increase in cytosolic mRFP, consistent with translocation of the probe from the transverse tubule into the cytosol, most likely reporting reduction of transverse tubule PtdIns(4,5)P_2 level. In the right graph of Fig. 10 B, the fluorescence intensity at a given location of the profile during the pulse (Fluo+50) was subtracted from the corresponding intensity after the pulse (Fluo−80(2)) and the difference plotted versus the post-pulse fluorescence intensity (Fluo−80(2)). The result is very similar to the one in the left graph, consistent with return of the probe to the transverse tubule membrane upon membrane repolarization.

This spatially distinct effect of strong depolarizing pulses on mRFP fluorescence is examined in an alternative way in Fig. 10 C; here, the analysis shown in Fig. 9 (B and C) was performed using either only the high intensity pixels in the initial/resting image (which should report a larger transverse tubule contribution) or only low intensity pixels (which should report a larger cytosolic contribution). Consistently, in response to the strong depolarizing pulses, pixels of high initial intensity tended to experience a transient decrease in fluorescence in contrast to pixels of low initial intensity. A similar analysis was successfully achieved in three out of four muscle fibers that were challenged by this same pulse protocol. Fig. 10 D shows the mean relative peak change in mRFP fluorescence versus membrane potential calculated using either all pixels in the images or using only high intensity or low intensity initial pixels. Collectively, these results appear very consistent with voltage-activated translocation of the PLCδ_1-PH probe from the triad into the cytosol, with a voltage dependence similar to that of Ci-VSP activation.

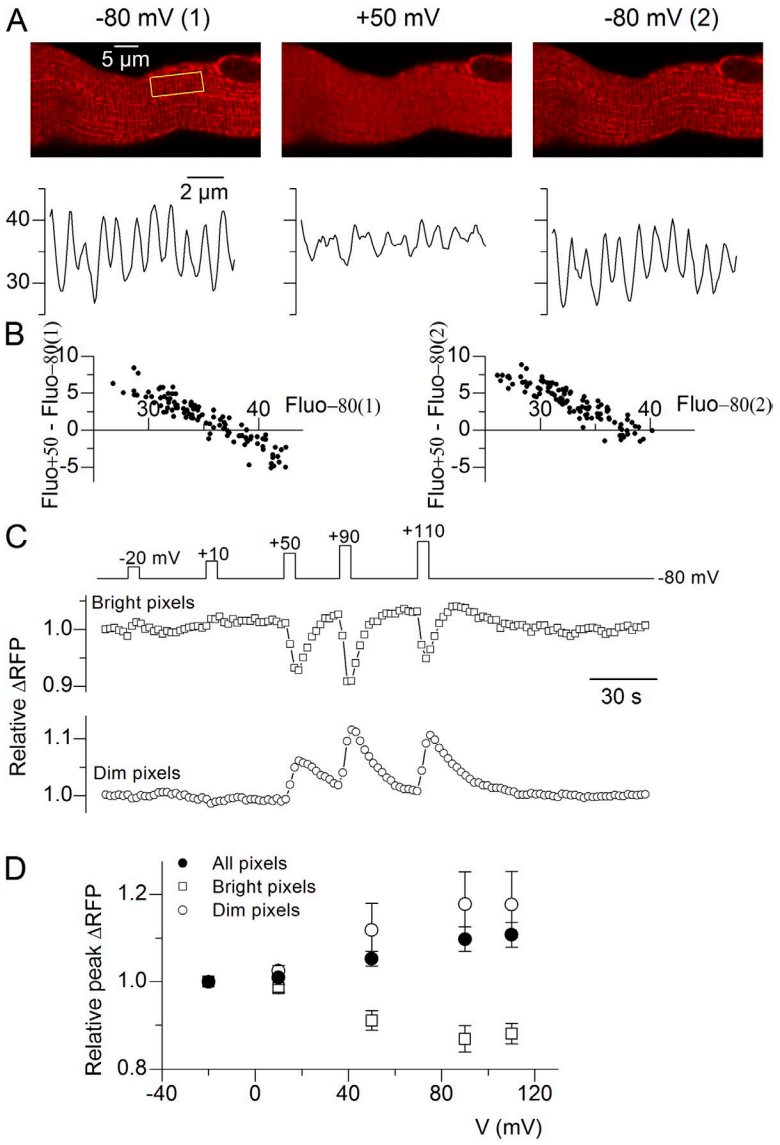

Figure 10. Spatially segregated distinct changes in PLCδ_1PH-mRFP fluorescence upon strong membrane depolarization in fibers expressing Ci-VSP. (A) Confocal images of a portion of a muscle fiber expressing Ci-VSP and PLCδ_1PH-mRFP. Images from left to right were taken before, during, and after a 5-s-long depolarizing pulse to 50 mV, respectively. The graph below each image shows the fluorescence intensity profile along the rectangular area highlighted in the image on the left. (B; left graph) Difference between the intensity at a given location of the fluorescence profile during the pulse (Fluo+50) and its corresponding intensity before the pulse (Fluo−80(1)) versus Fluo−80(1). (Right graph) Difference between the intensity at a given location of the fluorescence profile during the pulse (Fluo+50) and its corresponding intensity after the pulse (Fluo−80(2)) versus Fluo−80(2). (C) Result of the analysis similar to that shown in Fig. 9 C, except that pixels with high initial intensity and low initial intensity were separated; pixel selection was achieved by adjusting manually the threshold tool in ImageJ in the first image of the sequence. (D) Mean relative peak change in PLCδ_1PH-mRFP fluorescence versus membrane potential calculated from three fibers that experienced the pulse protocol shown in C; closed circles, open squares, and open circles correspond to values obtained using all, high intensity, and low intensity initial pixels, respectively. Error bars represent ± SEM.

One unclear feature of the mRFP signal is that if PLCδ$_1$-PH molecules simply translocate from membrane to cytosol, no change in the global fluorescence should occur. As there is no reason for the number of PH molecules available in the fibers to increase in response to the large depolarizing pulses, there has to be nonlinearity in the system that makes the fluorescence increase. We have no clear-cut explanation for this yet. There are two factors that may contribute to this effect. One possibility is that changes in the local microenvironment experienced by mRFP upon translocation from membrane to cytosol modify its fluorescence properties, as was suggested for PH constructs with CFP, YFP, or GFP (van der Wal et al., 2001), although the changes observed by these authors corresponded to a decreased intensity upon translocation to the cytosol. Another possibility is that the fluorescence intensity from the PH domain molecules bound to the transverse tubule membrane at rest underestimates its actual concentration; this could be enhanced by the fact that the confocal imaging system detects essentially the fluorescence from the cytosol, even in the regions of higher resting fluorescence, which we assume correspond to the transverse tubules.

Change in PtdIns(4,5)P_2 after Ci-VSP activation by a train of depolarizing steps

It was of specific interest to determine whether the pulse-train protocol that we used to assess the effect of VSP activation on voltage-activated Ca^{2+} release (Fig. 4) induced a detectable change of the PLCδ$_1$PH-mRFP signal. Fig. 11 A shows mRFP fluorescence traces taken successively on the same fiber while applying, from left to right, the test protocol, no pulse protocol, the control protocol, and the test protocol again. Fluorescence was measured using the line-scan mode of the microscope (1 line per 11.4 ms). In the absence of pulses and also during the control-pulse protocol, the fluorescence exhibited only a progressive decay. In contrast, the series of pulses to 100 mV during the test protocol were clearly associated with a transient increase of the fluorescence. The rightmost trace in Fig. 11 A was calculated by simply dividing the sum of the two traces taken during a test protocol by the sum of the two other traces. Fig. 11 B shows the mean (±SEM) change in fluorescence measured in four fibers during the test protocol: in each fiber, the fluorescence record during the test protocol was processed as in Fig. 11 A, using bracketing traces recorded while either applying no pulse and/or while applying a control protocol. Results clearly indicate the efficiency of the series of pulses to 100 mV to mobilize the PtdIns(4,5)P_2-binding probe.

DISCUSSION

We used VSP as a tool to deplete PtdIns(4,5)P_2 in the sarcolemma and transverse tubule membrane of skeletal muscle fibers. Results show that VSP can be expressed by in vivo electroporation in mouse muscle without disturbing the basic morphological and functional properties of the muscle fibers. VSP expresses and is active in the transverse tubule membrane of the transfected muscle fibers. PtdIns(4,5)P_2 visualized by expression of mRFP-tagged PLCδ$_1$PH domain also localizes to the transverse tubule membrane. Activating VSP alters the localization of the PLCδ$_1$PH domain in a way that is consistent with its translocation to the cytosol. Activating VSP reduces SR Ca^{2+} release during depolarizing pulses. This last point is the new message: PtdIns(4,5)P_2 depletion depresses calcium release.

Although an absolute quantification of the extent of VSP activation–induced PtdIns(4,5)P_2 depletion in the transverse tubule membrane was not possible with the mRFP probe, the quite extensive disappearance of the spatial distribution of the mRFP signal triggered by strong

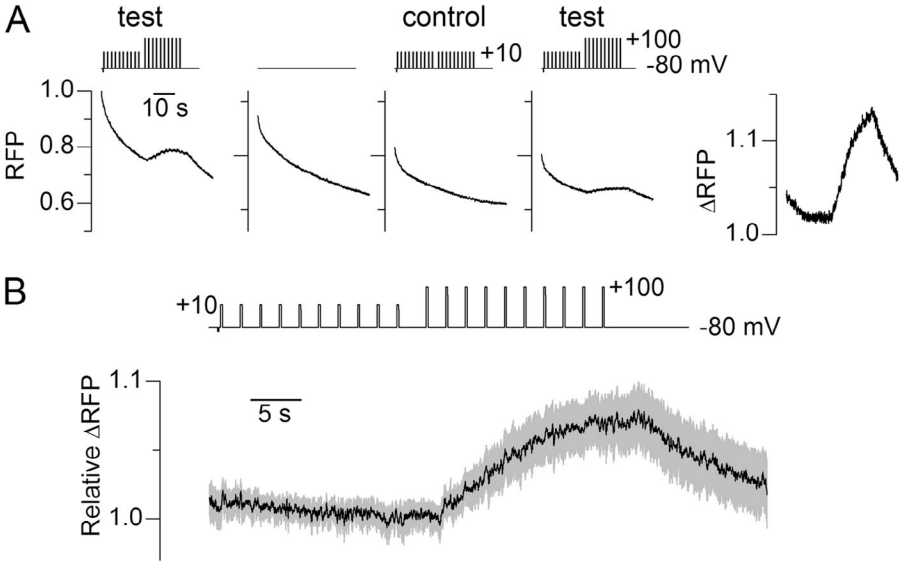

Figure 11. Changes in PLCδ$_1$PH-mRFP fluorescence in Ci-VSP–expressing fibers during the train of depolarizing steps protocol. (A) PLCδ$_1$PH-mRFP fluorescence detected in a fiber successively challenged by the above shown voltage-pulse protocols; fluorescence was measured in line-scan mode. The rightmost trace corresponds to the ratio of the sum of the two traces taken during a test train-pulse protocol and the sum of the two other traces. (B) Mean (±SEM; gray shading) change in fluorescence during the test protocol ($n = 4$); in each fiber, the fluorescence record during the test protocol was normalized by bracketing traces recorded while either applying no pulse or while applying a control protocol.

depolarizing pulses is likely to correlate with a substantial reduction of the membrane-bound PtdIns(4,5)P_2 level. One other quite remarkable feature of this signal is its transient nature with recovery occurring with a time constant in the 10-s range, which appears independent of the VSP-activating voltage. Assuming PtdIns(4)P to be the main PtdIns(4,5)P_2 precursor in the plasma membrane, this indicates that the transverse tubule membrane of muscle fibers is well equipped with PtdIns 5 kinase activity to face PtdIns(4,5)P_2 depletion and reconstitute the pool.

Upon depolarization VSPs dephosphorylate the 5′ position of PtdIns(3,4,5)P_3 and PtdIns(4,5)P_2 and the 3′ position of PtdIns(3,4)P_2 (Kurokawa et al., 2012). In the present conditions, we tend to favor PtdIns(4,5)P_2 as the active molecule because of its rich history of function in regulating ion channels and transporters in the plasma membrane of various cell types, and also because of our results with the PtdIns(4,5)P_2-selective PLCδ_1PH probe. However, we cannot exclude a possible contribution from the two other substrates.

Another point that is worth stressing is that although we assumed that VSP was negligibly activated during pulses to 20 mV, this was likely not entirely the case, specifically with Ci-VSP, which yielded the most negative voltage dependence. However, because our major aim was to compare Ca^{2+} release during strong VSP activation to Ca^{2+} release without (or with less) VSP activation in a same muscle fiber, Ca^{2+} release needed to be maximally activated with respect to its voltage dependence in both cases; so, pulses to 10 or 20 mV were required in the non-VSP–activating situation.

The question of how Ca^{2+} release can be affected by PtdIns(4,5)P_2 depletion is then the upcoming challenge. Although we are tempted to dismiss a role of PtdIns(4,5)P_2 as precursor of the Ca^{2+}-mobilizing molecule Ins(1,4,5)P_3 because of the lines of evidence denying a role for this pathway in the control of E-C coupling–related Ca^{2+} signals in differentiated muscle fibers (see Foster, 1994; Blaauw et al., 2012), we cannot unequivocally reject the possibility of a contribution of this process to the VSP effect we observe.

The alternative is to consider an interaction of PtdIns(4,5)P_2 with a protein partner of the E-C coupling machinery. Interestingly, in the 1990s several studies using skinned fibers, SR membrane preparations, and RyR channels incorporated into a phospholipid bilayer showed that RyR1 activity and Ca^{2+} release could be directly triggered or enhanced by PtdIns(4,5)P_2 (Kobayashi et al., 1989; Ogawa and Harafuji, 1989; Chu and Stefani, 1991; Ohizumi et al., 1999). Although no clear correlate was given as to how PtdIns(4,5)P_2 could act under physiological conditions, results emphasized that PtdIns(4,5)P_2 either would be active because it is present in the SR membrane, or could somehow be released from the transverse tubule to the SR membrane upon muscle stimulation (Chu and Stefani, 1991). Under our conditions, VSP activation depletes PtdIns(4,5)P_2 in the transverse tubule membrane, and the possibility that PtdIns(4,5)P_2 could rapidly shuttle from the transverse tubule to the SR terminal cisternae upon cell depolarization seems unlikely. Nevertheless, given the close apposition between the DHPR and RyR1, one could propose that PtdIns(4,5)P_2 may either interact with a cytoplasmic region of RyR1 that is close to the transverse tubule membrane, or sneak into the molecular interactions that make Cav1.1 control RyR1 opening.

Cav1.1 could be the potential target, as PtdIns(4,5)P_2 has been shown to regulate the activity of other voltage-gated Ca^{2+} channels (e.g., Suh et al., 2010), potentially through a dual interaction with a fatty acid–binding site on a transmembrane part of the channel and a cytoplasmic part of the channel (see Suh et al., 2012). Our present results provide no indication that Cav1.1 Ca^{2+} channel activity is strongly affected by VSP activation. However, it could still be that depletion of transverse tubule PtdIns(4,5)P_2 affects Cav1.1–RyR1 interaction in a subtle way that preserves the voltage-dependent Ca^{2+} channel activity.

Alternatively, PtdIns(4,5)P_2 could also be thought to act as a docking target for another protein capable of enhancing the efficiency of depolarization-induced SR Ca^{2+} release. For instance, annexin VI, which was initially presumed to modify the activity of the Ca^{2+} release channel from the SR luminal side, was then shown to be attached to transverse tubule membrane in isolated triads, likely because of its PtdIns(4,5)P_2-binding properties (Barrientos and Hidalgo, 2002). Also dysferlin, a transverse tubule membrane protein present at triadic junctions presumably in association with the DHPR, was recently shown to contribute to Ca^{2+} homeostasis (Kerr et al., 2013), and is also known to interact with PtdIns(4,5)P_2 (Therrien et al., 2009).

The modulation of Ca^{2+} release by transverse tubule PtdIns(4,5)P_2 level may be relevant under particular physiological or pathological conditions. PtdIns(4,5)P_2 is a substrate for phospholipase C and for type 1 PtdIns-3 kinase, making it an inescapable target in several signaling cascades; there is thus the possibility that specific conditions of activation of either or both of these enzymes does modify the transverse tubule PtdIns(4,5)P_2 content so as to modulate Ca^{2+} release. The plasma membrane level of PtdIns(4,5)P_2 was also shown to be increased by hyperosmolarity in several cell types including cardiac cells (Nasuhoglu et al., 2002), which may occur in skeletal muscle during high intensity exercise (Lindinger et al., 1992). The potential for alteration in phosphoinositide metabolism to trigger specific muscle diseases was demonstrated by the fact that deficiency in the phosphatidylinositol-phosphate Mtm1 is responsible for myotubular myopathy (Taylor et al., 2000). Interestingly, there is strong evidence that defective SR Ca^{2+} release is primarily involved in this

disease (Al-Qusairi et al., 2009; Rodríguez et al., 2014). Collectively, our results demonstrate the potential offered by expression of VSPs in adult muscle fibers to investigate signaling mechanisms dependent on plasma membrane phosphoinositides and suggest that voltage-activated SR Ca^{2+} release is enhanced by the presence of PtdIns(4,5)P_2 in the transverse tubule membrane.

We are grateful to Dr. Tamas Balla for providing us the PLCδ_1PH-mRFP construct. We thank Ms. Megumi Kobahashi for generating the GFP-tagged Dr-VSP construct; Thomas Loustau for performing early preliminary experiments; Jimmy Perrot for technical help; Bruno Allard for critical comments on the manuscript; and Bruno Allard, Pierre Charnet, and Norbert Weiss for helpful discussion.

This work was supported by grants from Centre National de la Recherche Scientifique and Université Lyon 1 to Centre de Génétique et de Physiologie Moléculaire et Cellulaire, and by a grant from Association Française contre les Myopathies to V. Jacquemond (AFM no. 15677).

The authors declare no competing financial interests.

Eduardo Ríos served as editor.

Submitted: 23 October 2014
Accepted: 5 March 2015

REFERENCES

Al-Qusairi, L., N. Weiss, A. Toussaint, C. Berbey, N. Messaddeq, C. Kretz, D. Sanoudou, A.H. Beggs, B. Allard, J.L. Mandel, et al. 2009. T-tubule disorganization and defective excitation-contraction coupling in muscle fibers lacking myotubularin lipid phosphatase. *Proc. Natl. Acad. Sci. USA.* 106:18763–18768. http://dx.doi.org/10.1073/pnas.0900705106

Barrientos, G., and C. Hidalgo. 2002. Annexin VI is attached to transverse-tubule membranes in isolated skeletal muscle triads. *J. Membr. Biol.* 188:163–173. http://dx.doi.org/10.1007/s00232-001-0179-x

Blaauw, B., P. Del Piccolo, L. Rodriguez, V.H. Hernandez Gonzalez, L. Agatea, F. Solagna, F. Mammano, T. Pozzan, and S. Schiaffino. 2012. No evidence for inositol 1,4,5-trisphosphate-dependent Ca^{2+} release in isolated fibers of adult mouse skeletal muscle. *J. Gen. Physiol.* 140:235–241. http://dx.doi.org/10.1085/jgp.201110747

Casas, M., R. Figueroa, G. Jorquera, M. Escobar, J. Molgó, and E. Jaimovich. 2010. IP_3-dependent, post-tetanic calcium transients induced by electrostimulation of adult skeletal muscle fibers. *J. Gen. Physiol.* 136:455–467. http://dx.doi.org/10.1085/jgp.200910397

Cheng, H., W.J. Lederer, and M.B. Cannell. 1993. Calcium sparks: elementary events underlying excitation-contraction coupling in heart muscle. *Science.* 262:740–744. http://dx.doi.org/10.1126/science.8235594

Chu, A., and E. Stefani. 1991. Phosphatidylinositol 4,5-bisphosphate-induced Ca^{2+} release from skeletal muscle sarcoplasmic reticulum terminal cisternal membranes. Ca^{2+} flux and single channel studies. *J. Biol. Chem.* 266:7699–7705.

Collet, C., L. Csernoch, and V. Jacquemond. 2003. Intramembrane charge movement and L-type calcium current in skeletal muscle fibers isolated from control and mdx mice. *Biophys. J.* 84:251–265. http://dx.doi.org/10.1016/S0006-3495(03)74846-2

Collet, C., S. Pouvreau, L. Csernoch, B. Allard, and V. Jacquemond. 2004. Calcium signaling in isolated skeletal muscle fibers investigated under "silicone voltage-clamp" conditions. *Cell Biochem. Biophys.* 40:225–236. http://dx.doi.org/10.1385/CBB:40:2:225

Dulhunty, A.F. 2006. Excitation-contraction coupling from the 1950s into the new millennium. *Clin. Exp. Pharmacol. Physiol.* 33:763–772. http://dx.doi.org/10.1111/j.1440-1681.2006.04441.x

Foster, P.S. 1994. The role of phosphoinositide metabolism in Ca^{2+} signalling of skeletal muscle cells. *Int. J. Biochem.* 26:449–468. http://dx.doi.org/10.1016/0020-711X(94)90001-9

Hossain, M.I., H. Iwasaki, Y. Okochi, M. Chahine, S. Higashijima, K. Nagayama, and Y. Okamura. 2008. Enzyme domain affects the movement of the voltage sensor in ascidian and zebrafish voltage-sensing phosphatases. *J. Biol. Chem.* 283:18248–18259. http://dx.doi.org/10.1074/jbc.M706184200

Jacquemond, V. 1997. Indo-1 fluorescence signals elicited by membrane depolarization in enzymatically isolated mouse skeletal muscle fibers. *Biophys. J.* 73:920–928. http://dx.doi.org/10.1016/S0006-3495(97)78124-4

Jorquera, G., F. Altamirano, A. Contreras-Ferrat, G. Almarza, S. Buvinic, V. Jacquemond, E. Jaimovich, and M. Casas. 2013. Cav1.1 controls frequency-dependent events regulating adult skeletal muscle plasticity. *J. Cell Sci.* 126:1189–1198. http://dx.doi.org/10.1242/jcs.116855

Kerr, J.P., A.P. Ziman, A.L. Mueller, J.M. Muriel, E. Kleinhans-Welte, J.D. Gumerson, S.S. Vogel, C.W. Ward, J.A. Roche, and R.J. Bloch. 2013. Dysferlin stabilizes stress-induced Ca^{2+} signaling in the transverse tubule membrane. *Proc. Natl. Acad. Sci. USA.* 110:20831–20836. http://dx.doi.org/10.1073/pnas.1307960110

Kobayashi, M., A. Muroyama, and Y. Ohizumi. 1989. Phosphatidylinositol 4,5-bisphosphate enhances calcium release from sarcoplasmic reticulum of skeletal muscle. *Biochem. Biophys. Res. Commun.* 163:1487–1491. http://dx.doi.org/10.1016/0006-291X(89)91147-9

Kurokawa, T., S. Takasuga, S. Sakata, S. Yamaguchi, S. Horie, K.J. Homma, T. Sasaki, and Y. Okamura. 2012. 3′ Phosphatase activity toward phosphatidylinositol 3,4-bisphosphate [PI(3,4)P2] by voltage-sensing phosphatase (VSP). *Proc. Natl. Acad. Sci. USA.* 109:10089–10094. http://dx.doi.org/10.1073/pnas.1203799109

Lefebvre, R., C. Legrand, E. González-Rodríguez, L. Groom, R.T. Dirksen, and V. Jacquemond. 2011. Defects in Ca^{2+} release associated with local expression of pathological ryanodine receptors in mouse muscle fibres. *J. Physiol.* 589:5361–5382. http://dx.doi.org/10.1113/jphysiol.2011.216408

Lefebvre, R., C. Legrand, L. Groom, R.T. Dirksen, and V. Jacquemond. 2013. Ca^{2+} release in muscle fibers expressing R4892W and G4896V type 1 ryanodine receptor disease mutants. *PLoS ONE.* 8:e54042. http://dx.doi.org/10.1371/journal.pone.0054042

Legrand, C., E. Giacomello, C. Berthier, B. Allard, V. Sorrentino, and V. Jacquemond. 2008. Spontaneous and voltage-activated Ca^{2+} release in adult mouse skeletal muscle fibres expressing the type 3 ryanodine receptor. *J. Physiol.* 586:441–457. http://dx.doi.org/10.1113/jphysiol.2007.145862

Lindinger, M.I., G.J. Heigenhauser, R.S. McKelvie, and N.L. Jones. 1992. Blood ion regulation during repeated maximal exercise and recovery in humans. *Am. J. Physiol.* 262:R126–R136.

Melzer, W., A. Herrmann-Frank, and H.C. Lüttgau. 1995. The role of Ca^{2+} ions in excitation-contraction coupling of skeletal muscle fibres. *Biochim. Biophys. Acta.* 1241:59–116. http://dx.doi.org/10.1016/0304-4157(94)00014-5

Murata, Y., H. Iwasaki, M. Sasaki, K. Inaba, and Y. Okamura. 2005. Phosphoinositide phosphatase activity coupled to an intrinsic voltage sensor. *Nature.* 435:1239–1243. http://dx.doi.org/10.1038/nature03650

Nasuhoglu, C., S. Feng, Y. Mao, I. Shammat, M. Yamamato, S. Earnest, M. Lemmon, and D.W. Hilgemann. 2002. Modulation of cardiac PIP_2 by cardioactive hormones and other physiologically relevant interventions. *Am. J. Physiol. Cell Physiol.* 283:C223–C234. http://dx.doi.org/10.1152/ajpcell.00486.2001

Ogawa, Y., and H. Harafuji. 1989. Ca-release by phosphoinositides from sarcoplasmic reticulum of frog skeletal muscle. *J. Biochem.* 106:864–867.

Ohizumi, Y., Y. Hirata, A. Suzuki, and M. Kobayashi. 1999. Two novel types of calcium release from skeletal sarcoplasmic reticulum by phosphatidylinositol 4,5-biphosphate. *Can. J. Physiol. Pharmacol.* 77:276–285. http://dx.doi.org/10.1139/y99-017

Pouvreau, S., and V. Jacquemond. 2005. Nitric oxide synthase inhibition affects sarcoplasmic reticulum Ca^{2+} release in skeletal muscle fibres from mouse. *J. Physiol.* 567:815–828. http://dx.doi.org/10.1113/jphysiol.2005.089599

Pouvreau, S., L. Csernoch, B. Allard, J.M. Sabatier, M. De Waard, M. Ronjat, and V. Jacquemond. 2006. Transient loss of voltage control of Ca^{2+} release in the presence of maurocalcine in skeletal muscle. *Biophys. J.* 91:2206–2215. http://dx.doi.org/10.1529/biophysj.105.078089

Ríos, E., G. Pizarro, and E. Stefani. 1992. Charge movement and the nature of signal transduction in skeletal muscle excitation-contraction coupling. *Annu. Rev. Physiol.* 54:109–133. http://dx.doi.org/10.1146/annurev.ph.54.030192.000545

Rodríguez, E.G., R. Lefebvre, D. Bodnár, C. Legrand, P. Szentesi, J. Vincze, K. Poulard, J. Bertrand-Michel, L. Csernoch, A. Buj-Bello, and V. Jacquemond. 2014. Phosphoinositide substrates of myotubularin affect voltage-activated Ca^{2+} release in skeletal muscle. *Pflugers Arch.* 466:973–985. http://dx.doi.org/10.1007/s00424-013-1346-5

Sakata, S., M.I. Hossain, and Y. Okamura. 2011. Coupling of the phosphatase activity of Ci-VSP to its voltage sensor activity over the entire range of voltage sensitivity. *J. Physiol.* 589:2687–2705. http://dx.doi.org/10.1113/jphysiol.2011.208165

Schneider, M.F. 1994. Control of calcium release in functioning skeletal muscle fibers. *Annu. Rev. Physiol.* 56:463–484. http://dx.doi.org/10.1146/annurev.ph.56.030194.002335

Stauffer, T.P., S. Ahn, and T. Meyer. 1998. Receptor-induced transient reduction in plasma membrane PtdIns(4,5)P2 concentration monitored in living cells. *Curr. Biol.* 8:343–346. http://dx.doi.org/10.1016/S0960-9822(98)70135-6

Suh, B.C., K. Leal, and B. Hille. 2010. Modulation of high-voltage activated Ca^{2+} channels by membrane phosphatidylinositol 4,5-bisphosphate. *Neuron.* 67:224–238. http://dx.doi.org/10.1016/j.neuron.2010.07.001

Suh, B.C., D.I. Kim, B.H. Falkenburger, and B. Hille. 2012. Membrane-localized β-subunits alter the PIP2 regulation of high-voltage activated Ca^{2+} channels. *Proc. Natl. Acad. Sci. USA.* 109:3161–3166. http://dx.doi.org/10.1073/pnas.1121434109

Taylor, G.S., T. Maehama, and J.E. Dixon. 2000. Myotubularin, a protein tyrosine phosphatase mutated in myotubular myopathy, dephosphorylates the lipid second messenger, phosphatidylinositol 3-phosphate. *Proc. Natl. Acad. Sci. USA.* 97:8910–8915. http://dx.doi.org/10.1073/pnas.160255697

Therrien, C., S. Di Fulvio, S. Pickles, and M. Sinnreich. 2009. Characterization of lipid binding specificities of dysferlin C2 domains reveals novel interactions with phosphoinositides. *Biochemistry.* 48:2377–2384. http://dx.doi.org/10.1021/bi802242r

Tjondrokoesoemo, A., N. Li, P.H. Lin, Z. Pan, C.J. Ferrante, N. Shirokova, M. Brotto, N. Weisleder, and J. Ma. 2013. Type 1 inositol (1,4,5)-trisphosphate receptor activates ryanodine receptor 1 to mediate calcium spark signaling in adult mammalian skeletal muscle. *J. Biol. Chem.* 288:2103–2109. http://dx.doi.org/10.1074/jbc.M112.425975

Treves, S., M. Vukcevic, M. Maj, R. Thurnheer, B. Mosca, and F. Zorzato. 2009. Minor sarcoplasmic reticulum membrane components that modulate excitation-contraction coupling in striated muscles. *J. Physiol.* 587:3071–3079. http://dx.doi.org/10.1113/jphysiol.2009.171876

van der Wal, J., R. Habets, P. Várnai, T. Balla, and K. Jalink. 2001. Monitoring agonist-induced phospholipase C activation in live cells by fluorescence resonance energy transfer. *J. Biol. Chem.* 276:15337–15344. http://dx.doi.org/10.1074/jbc.M007194200

Várnai, P., and T. Balla. 1998. Visualization of phosphoinositides that bind pleckstrin homology domains: Calcium- and agonist-induced dynamic changes and relationship to myo-[3H]inositol-labeled phosphoinositide pools. *J. Cell Biol.* 143:501–510. http://dx.doi.org/10.1083/jcb.143.2.501

Weiss, N., C. Legrand, S. Pouvreau, H. Bichraoui, B. Allard, G.W. Zamponi, M. De Waard, and V. Jacquemond. 2010. In vivo expression of G-protein beta1gamma2 dimer in adult mouse skeletal muscle alters L-type calcium current and excitation-contraction coupling. *J. Physiol.* 588:2945–2960. http://dx.doi.org/10.1113/jphysiol.2010.191593

Yamaguchi, S., T. Kurokawa, I. Taira, N. Aoki, S. Sakata, Y. Okamura, and K.J. Homma. 2014. Potential role of voltage-sensing phosphatases in regulation of cell structure through the production of $PI(3,4)P_2$. *J. Cell. Physiol.* 229:422–433. http://dx.doi.org/10.1002/jcp.24463